Optimization of gaseous nitriding of steels by multi-physics modelling

Dr. Sébastien JÉGOU, Prof. Laurent BARRALLIER
MSMP Laboratory, Arts et Métiers ParisTech, Aix-en-Provence, France
sebastien.jegou@ensam.eu, laurent.barrallier@ensam.eu

Dr. Guillaume FALLOT
Airbus Helicopters, Marignane, France
guillaume.fallot@airbus.com

Abstract

Gaseous nitriding is controlled by temperature, time and surface nitrogen potential. Tuning these parameters lead to the expected mechanical properties (hardness, residual stresses) and durability of treated mechanical parts. In this paper, a methodology is proposed to optimize nitriding parameters by using a multi-physics modelling of the nitriding treatment (microstructure, diffusion/precipitation mechanisms, hardness and residual stress generation). This model is particularly suited to the diffusion layer and does not apply to the compound layer. The scope concerns low-alloyed carbon steels and gaseous nitriding. The role of carbon is established and taken into account in the proposed methodology.

Introduction

High service loads, weight and cost reductions have been requesting more and more efficiency from power transmission. Process design and modelling have naturally raised significant importance in aeronautic and automotive industries in order to optimize the conception of new and complex mechanical parts.

In case of surface treatments, modelling may help optimizing process parameters in order to achieve the case depth as well as microstructure that avoid case cracking, and predicting residual stress gradients for fatigue resistance and/or macroscopic volume change (or deformation of mechanical parts) calculation. Optimization of subsequent machining may be performed in order to full fill both the final quotes of the mechanical part and desired surface mechanical properties.

Among thermochemical surface treatments of steels, gaseous nitriding is widely used because it involves low distortions of treated parts due to a lower treatment temperature (450 to 590 °C associated to slow cooling to room temperature) compared to carburizing (around 900 °C and then quenched) [1]. In return, the diffusion process at such low temperature is significantly drop off and, because of associated with phase transformations, may induce detrimental microstructure for either residual stress generation or crack propagation if not well controlled [2-4].

In case of binary iron-based alloys, gaseous nitriding is well described [5-11]. The main feature is the diffusion of nitrogen in a ferritic matrix (α-Fe). Absorption of nitrogen atoms from the outer NH_3-rich atmosphere leads to the formation of a compound layer, composed of ε-$Fe_{2-3}N$ and/or γ'-Fe_4N, followed by a diffusion layer, composed of alloying elements nitrides MN (M = Cr, V, Mo…) finely dispersed into a ferritic matrix. For carbon iron-based alloys, the diffusion layer is also characterized by the precipitation of cementite Fe_3C from the transformation of initial carbides $M_{23}C_6/M_7C_3$ [12-13]. A co-diffusion of carbon also occurs that makes more complex phase transformations kinetics at the nitrogen diffusion front where an enrichment of carbon is commonly observed [2,14]. The kinetic of the compound layer formation is more or less affected depending on the NH_3-rich atmosphere leading to mainly decarburizing of the material at low nitriding potential K_N or carbon enrichment of the compound layer at high nitriding potential [15]. Modelling of the process becomes thus complex and only few authors introduced the diffusion of carbon into modelling. Torchane *et al.* studied the influence of carbon on the kinetics of formation of the compound layer in case of ternary Fe-C-N material [16]. Depouhon *et al.* proposed a 3D modelling that allows prediction of macroscopic volume change of treated part but based on inverse fitting of diffusion and residual stress gradients in order to determine the diffusion (nitrogen and carbon) and precipitation kinetics parameters of a given treated material [17].

Based on previous developments by the present authors, this work aims to compare experimental results with a model that is able to deal with the optimization of gaseous nitriding treatment of carbon iron-based alloys [18-23]. Comparisons are performed according to several nitriding conditions (time, temperature, nitriding potential) on an industrial 33CrMoV12-9 steel grade [3].

Experimental Methods

The material of the present study is an industrial nitriding steel grade 33CrMoV12-9. Its composition is given in Table 1. Samples of 17×13×5 mm^3 were austenitized at 950 °C during 30 min and oil quenched. Annealing was performed at 590 °C during 2.5 h prior to nitriding.

Table 1: Chemical composition of the studied 33CrMoV12-9 steel grade.

Composition (wt.%)					
C	**Cr**	**Mo**	**V**	**Mn**	**Fe**
0.318	2.97	0.84	0.28	0.55	balance

Gaseous nitriding was performed in a SETSYS Evolution thermogravimetric analyser from Setaram Instrumentation. The temperature of nitriding was set to 550 °C whereas the duration and potential of nitriding were varied from 2.5 to 30 h and 0.33 to 13.77 atm$^{-1/2}$ respectively. The nitriding atmosphere was composed of a gas mixture of NH_3-N_2-H_2 using a flow rate in the furnace of 200 mL.min^{-1}.

The determination of nitrogen and carbon contents were achieved by optical emission spectrometry using a Spectro SPECTROMAXx MX5M BT. Four analyses are performed on four different areas (of nearly 0.5 mm diameter each by 30 µm in depth) on each treated surface. Depth profiling is obtained by successive mechanical grinding until elimination of previous sparks. Layer removal was controlled by dial indicator.

Image analysis was carried out in order to determine the surface fraction of cementite Fe_3C at grain boundaries of prior austenite. To this purpose, observations were performed on a JEOL 7001F scanning electron microscope (SEM) operating at 15 kV and equipped with an energy-dispersive X-ray detection system (EDX). Image analyses were performed on backscattered electron micrographies due to a very good Z contrast between the matrix and cementite at grain boundaries. Each image was cut in slices of 20 µm for in-depth profiling.

Hardness-depth profiles were obtained using a Leica VMHT device with a load of 2 N during 15 s. The effective depth of nitriding was industrially defined as the core hardness plus 100 HV 0.2.

Modelling of nitriding

The present modelling of nitriding is defined in one direction perpendicular to the nitrided surface and based on the coupling of diffusion in solid solution in the ferritic matrix using Fick's laws and precipitation under thermodynamic equilibrium assumption using Thermo-Calc software (version 4.0 [24] and TC-API version 7.0 [25]). This approach allows estimation of the nitrogen and carbon contents as well as the chemical composition and volume fraction of phases through the case. Calculations are performed at the nitriding temperature using Thermo-Calc Software TCFE7 Steels/Fe-alloys database version 7 [26]. From the volume fraction of each phase at each depth as well as the calculation of the volume change accompanying phase transformations, it follows that the gradient of residual stresses can be determined based on a self-consistent micro-mechanical modelling. The next sessions will only focus on diffusion and precipitation calculations. Details and parameters of the model are given elsewhere in the literature [18-23].

It has to be noticed that the model does not apply to the formation of the compound layer. However it will be shown in the next session that the growth of the diffusion layer is governed by its interface with the compound layer due to fast growth kinetics. Surface boundary conditions of the model were consequently set up from experiments to values at this interface by assuming fast establishment of a steady state of nitriding. The chemical contents of nitrogen and carbon are then set constant and equal either to 2 wt.%N and 0.2 wt.%C

for high nitriding potential ($K_N > 0.33$ atm$^{-1/2}$) or 1.2 wt.%N and 0.05 wt.%C for low nitriding potential ($K_N < 0.33$ atm$^{-1/2}$).

Results

Nitrogen and carbon content in-depth profiles indicate a common trend. The longer the nitriding the deeper the case thickness is for given temperature and nitriding potential (Fig. 1). Carbon exhibits a typical co-diffusion that is characterized by, in one hand, an enrichment toward the nitrogen diffusion front and, in an other hand, a decarburization at the gas/solid interface followed by an enrichment of the compound layer for long nitriding (Fig. 2).
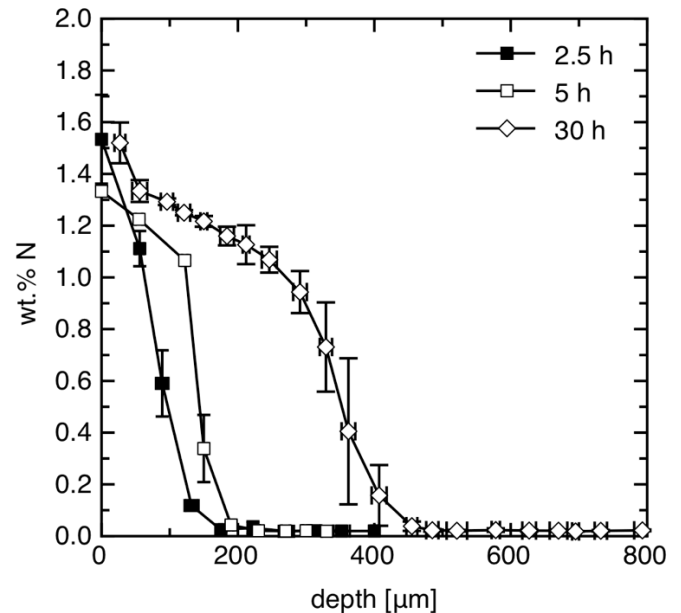

Figure 1: Nitrogen content in-depth profiles from OES analyses of a 33CrMoV12-9 steel nitrided at 550 °C and 3.65 atm$^{-1/2}$.

The evolutions of the nitrogen and carbon content in-depth profiles with the nitriding potential show that the nitrogen enrichment and decarburization of the case are strongly limited by nitriding conditions (Fig. 3 and 4). At $K_N = 0.33$ atm$^{-1/2}$ and 550 °C, the nitrogen diffusion and enrichment are non-negligibly decreased (Fig. 3). Low nitriding potential also involves deeper surface decarburization up to 100 µm below the surface against only 30 µm for higher potentials (Fig. 4).

SEM observations shows that nitriding at a low potential of $K_N = 0.33$ atm$^{-1/2}$ at 550 °C during 30 h induces no growth of a compound layer (Fig. 5.a). In the opposite, a compound layer of 11 µm thick developed at 550 °C at $K_N = 3.65$ atm$^{-1/2}$ after only 2.5 h (Fig. 5.b).

The evolution of the hardness in-depth profiles with nitriding conditions correlate observations from nitrogen content profiles (Fig. 6 and 7). The hardness levels and extent of in-depth profiles are directly related to the nitrogen diffusion and amount reacting with alloying elements to form alloying elements nitrides MN.
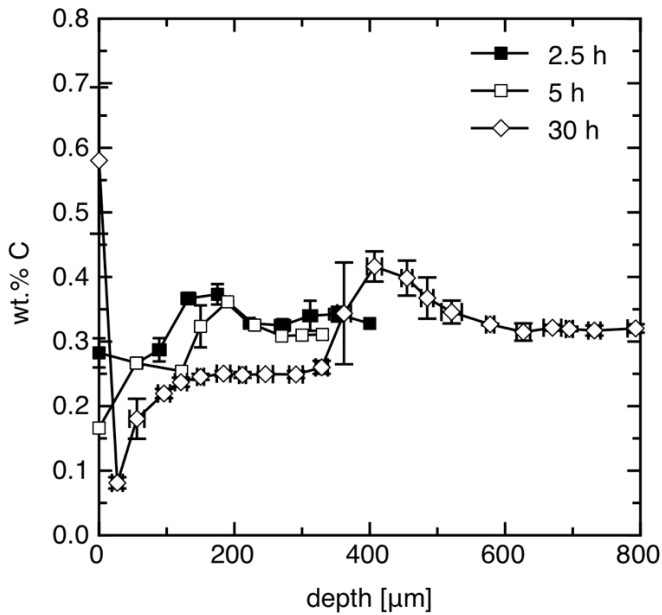
Figure 2: Carbon content in-depth profiles from OES analyses of a 33CrMoV12-9 steel nitrided at 550 °C and 3.65 atm$^{-1/2}$.
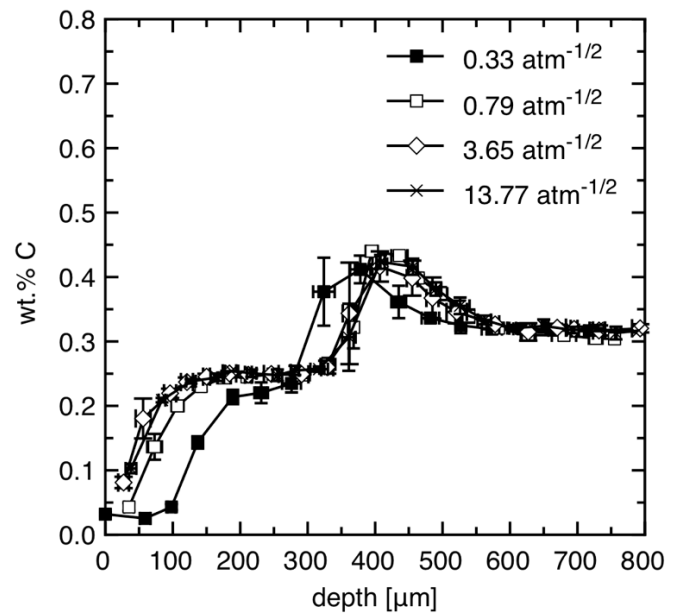

Figure 4: Carbon content in-depth profiles from OES analyses of a 33CrMoV12-9 steel nitrided at 550 °C during 30 h.

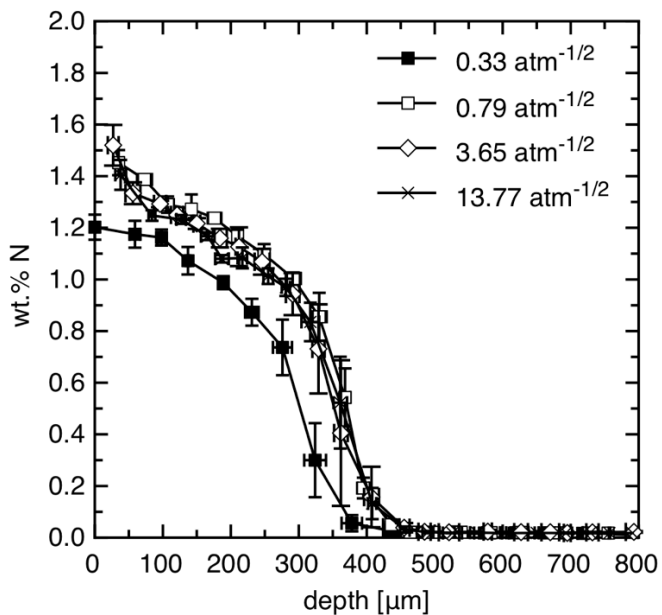
Figure 3: Nitrogen content in-depth profiles from OES analyses of a 33CrMoV12-9 steel nitrided at 550 °C during 30 h.
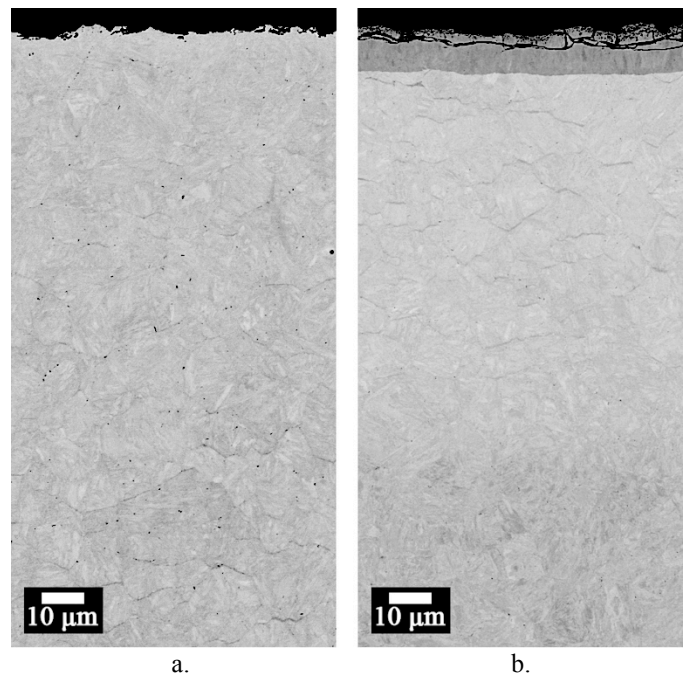

a.   b.

Figure 5: SEM micrographies of a 33CrMoV12-9 steel nitrided at 550 °C and (a.) Kn = 0.33 atm$^{-1/2}$ and (b.) Kn = 0.33 atm$^{-1/2}$ during 30 h.
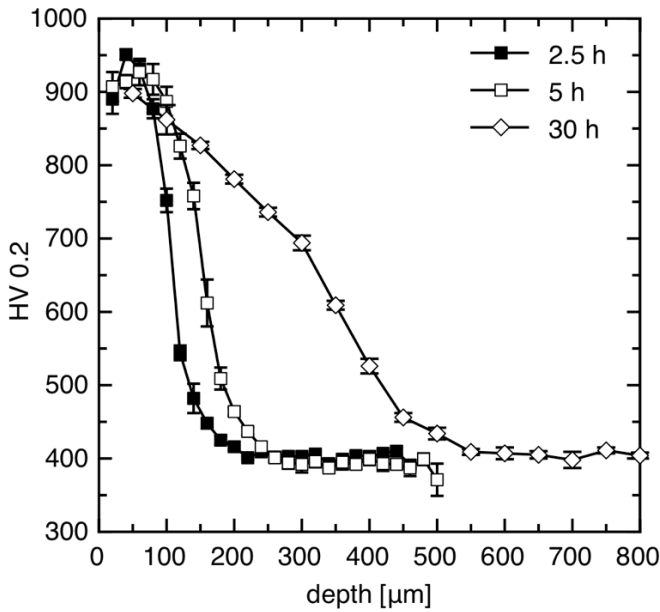
Figure 6: Hardness in-depth profiles of a 33CrMoV12-9 steel nitrided at 550 °C and 3.65 atm$^{-1/2}$.
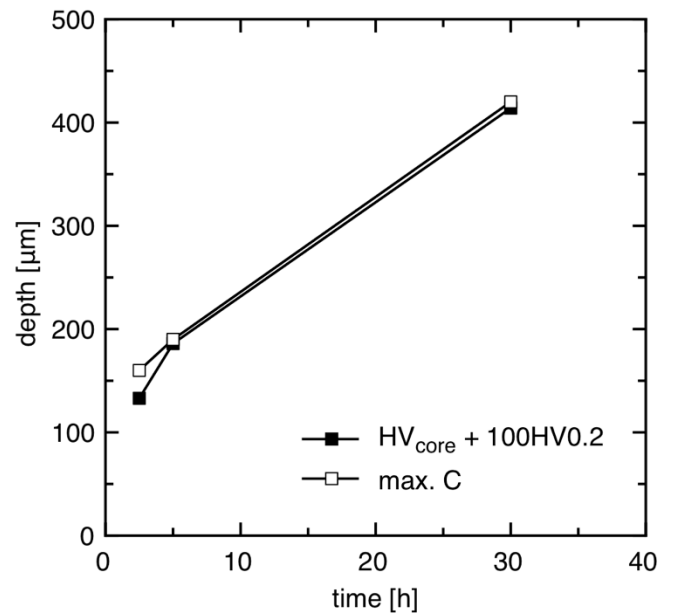

Figure 8: Relation between the effective depth and the location of the maximum carbon content of a 33CrMoV12-9 steel nitrided at 550 °C and 3.65 atm$^{-1/2}$. The effective depth of nitriding is defined as the core hardness plus 100 HV 0.2.
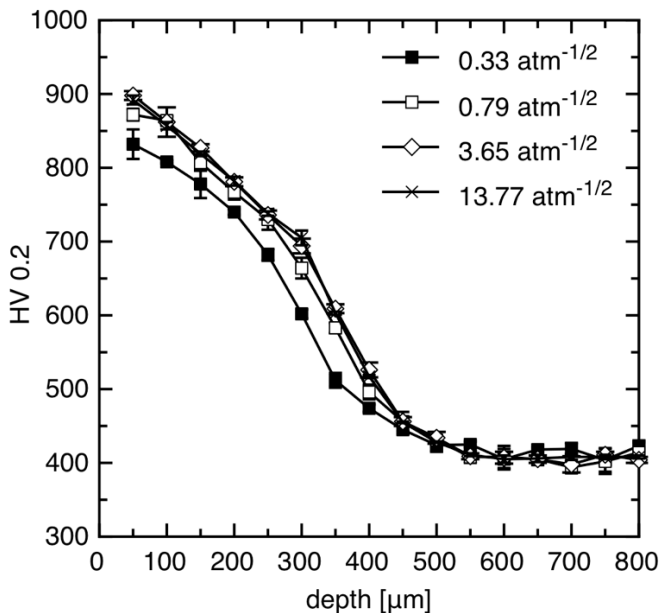

Figure 7: Hardness in-depth profiles of a 33CrMoV12-9 steel nitrided at 550 °C during 30 h.
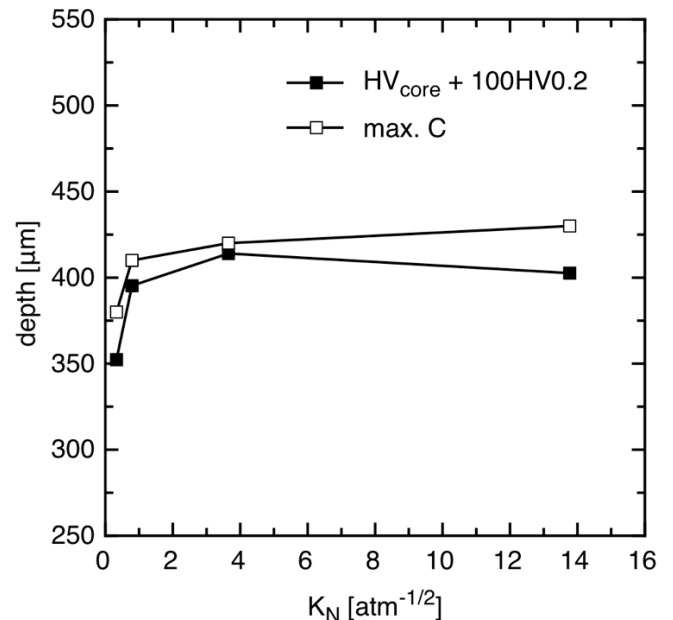

Figure 9: Relation between the effective depth and the location of the maximum carbon content of a 33CrMoV12-9 steel nitrided at 550 °C during 30 h. The effective depth of nitriding is defined as the core hardness plus 100 HV 0.2.

Experimental observations show that the decarburization and growth of the diffusion layer are governed by the formation of a compound layer. The establishment of a steady state occurs in the first few hours at 550 °C and K_N = 3.65 atm$^{-1/2}$.
Plotting the effective depth of nitriding (defined as core hardness plus 100 HV 0.2) and depth where the maximum of carbon is encountered at the nitrogen diffusion front against the nitriding conditions shows a similar trend that is linear with time (Fig. 8) and nearly constant with the nitriding potential (K_N > 0.33 atm$^{-1/2}$) enabling growth of a compound layer (Fig. 9).

Comparisons with the modelling of nitriding at 550 °C and several times of treatment are given in Figures 10 and 11 respectively. Good correlations are obtained for both nitrogen and carbon. Sharp interface between the nitrogen diffusion front and the core are given by the model (Fig. 11). The carbon enrichment is also largely overestimated at the nitrogen

diffusion front. They are related to the thermodynamics equilibrium assumption of the present model that is, by definition, not able to accurately track complex precipitation kinetics associated to strong diffusion gradients of both nitrogen and carbon. Results were obtained after setting up surface boundary conditions of nitrogen and carbon to fix values close to experimental contents at the outer surface for low nitriding potentials ($K_N < 0.33$ atm$^{-1/2}$ in the present case) or at the interface between the compound and diffusion layer (see § "Modelling of nitriding"). It rests on the observed fast establishment of a compound layer and steady state.
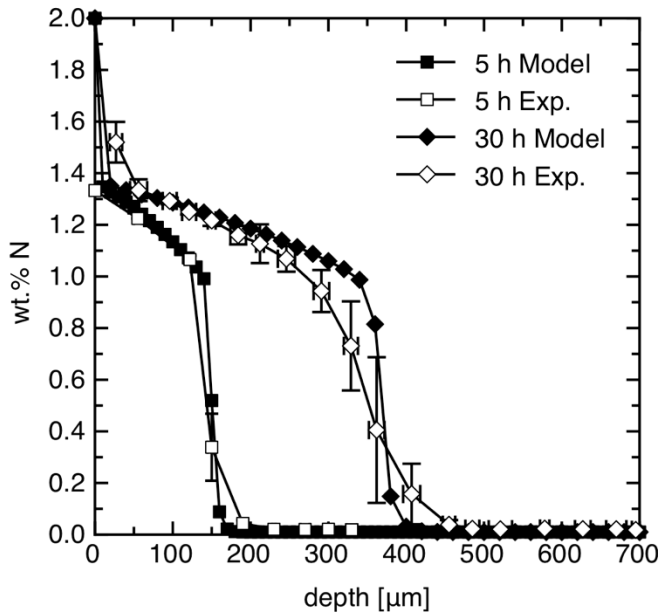

Figure 10: Comparisons between experimental and simulated nitrogen in-depths profiles of a 33CrMoV12-9 steel nitrided at 550 °C and 3.65 atm$^{-1/2}$.

Figure 12 gives a comparison between experimental and modelling content profiles in the case of a low nitriding potential that does not involve the growth of compound layer ($K_N = 0.33$ atm$^{-1/2}$). As previously, good correlations are obtained with the same limitations due to the thermodynamics equilibrium assumption. Comparisons between the depth where the maximum carbon content is found against time of nitriding from experiments and modelling are in good agreements (Fig. 13).

An interest in the present modelling also lies in the calculation of the volume fraction of each phase according to the diffusion of nitrogen and carbon. Figures 14 and 15 give the volume fraction of cementite Fe₃C as a function of the depth given by the model for two kinds of nitriding conditions (low and high nitrogen potentials). The calculated volume fraction of cementite is in good agreements with the surface fraction of cementite at grain boundaries of prior austenite grains measured by SEM image analysis.
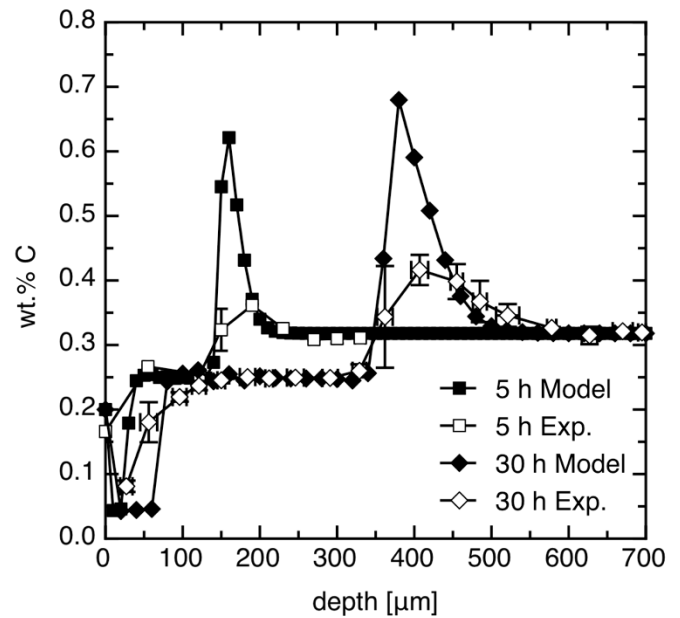

Figure 11: Comparisons between experimental and simulated carbon in-depths profiles of a 33CrMoV12-9 steel nitrided at 550 °C and 3.65 atm$^{-1/2}$.
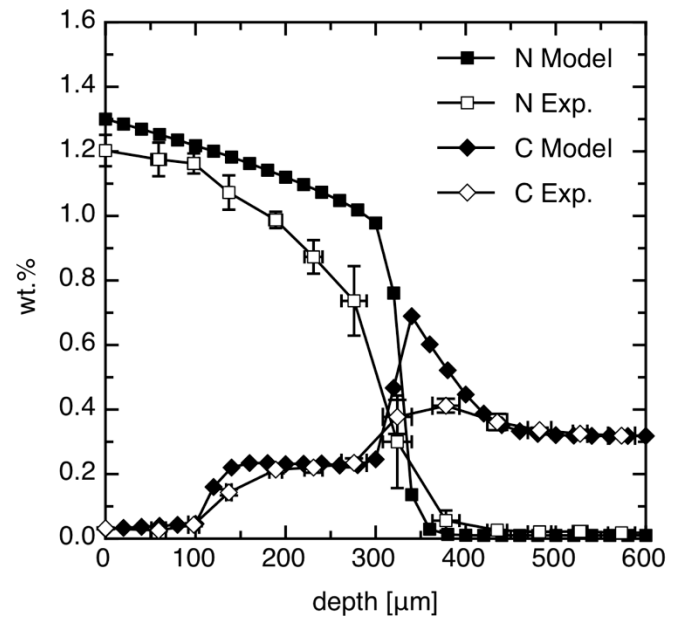

Figure 12: Comparisons between experimental and simulated nitrogen and carbon in-depths profiles of a 33CrMoV12-9 steel nitrided at 550 °C and 0.33 atm$^{-1/2}$ during 30 h.
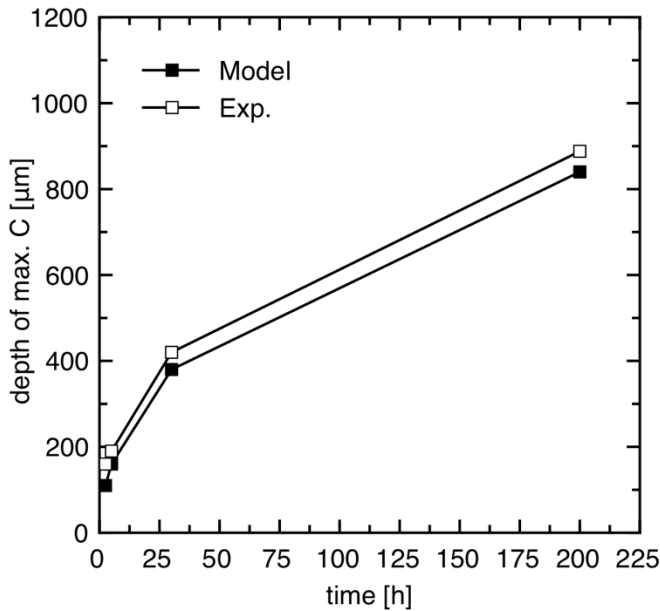
Figure 13: Comparisons between experimental and simulated depths corresponding to the maximum carbon content of a 33CrMoV12-9 steel nitrided at 550 °C and 3.65 atm$^{-1/2}$.
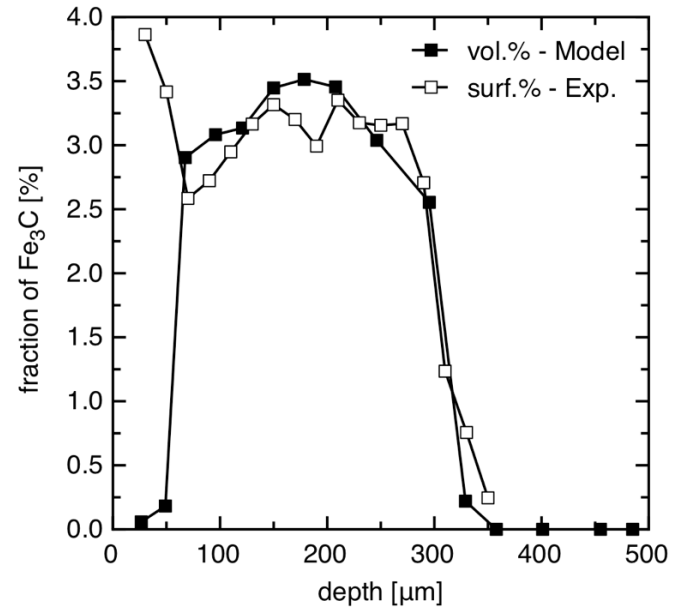

Figure 14: Comparisons between experimental and simulated fraction of cementite Fe₃C of a 33CrMoV12-9 steel nitrided at 550 °C and 0.33 atm$^{-1/2}$ during 30 h.

Figure 15: Comparisons between experimental and simulated fraction of cementite Fe₃C of a 33CrMoV12-9 steel nitrided at 550 °C and 3.65 atm$^{-1/2}$ during 30 h.

Discussion

Based on diffusion (Fick's laws) of both nitrogen and carbon in solid solution of a ferritic matrix and precipitation from thermodynamics calculation (Thermo-Calc package), the present model shows that a good prediction of the effective depth of nitriding as well as the fraction of phases (cementite) is obtained in case of an industrial grade dedicated to nitriding. It has to be noticed that only nitrogen and carbon surface boundary conditions were set up from experimental chemical analysis since gas/solid interactions and growth of the compound layer are not modelled. Discrepancies, mainly at the nitrogen diffusion front, are explained by the thermodynamics equilibrium assumption used for taking into account phase transformations. By definition, such assumption is not able to describe complex phase transformation kinetics due to nitrogen and carbon diffusion.

From Figures 8, 9 and 13, it follows that the nitriding conditions for a given effective depth (defined from hardness profiles) may be estimated from the present modelling based on the diffusion of carbon and its enrichment at the nitrogen diffusion front. For instance, assuming nitriding of a 33CrMoV12-9 steel at 520 °C, and using the same parameters (boundary conditions, nitrogen and carbon diffusion coefficients) set up fro nitriding at 550 °C, Figure 16 shows that good agreements are obtained between the experimental effective depth and depth where the maximum carbon content is located.

The method proposed of determining the effective depth of nitriding based on estimating the depth of the maximum content of carbon from modelling allows optimization of the treatment parameters in a process where the effective depth is the easiest measurable parameter. Coupling with residual
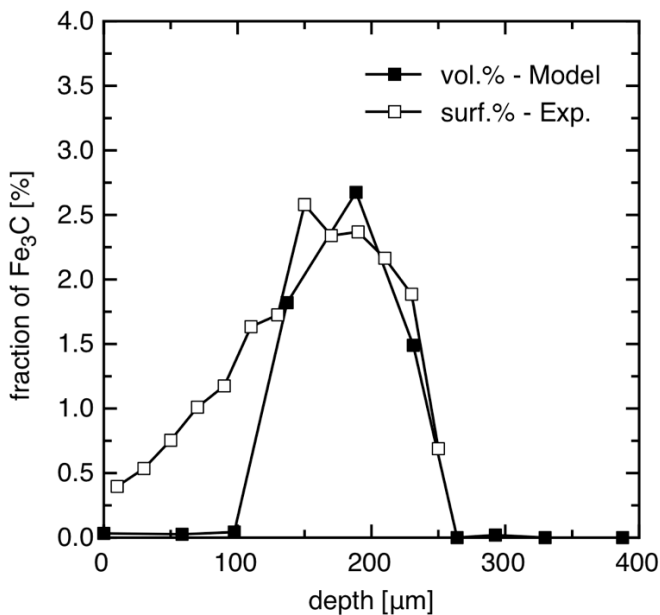
stress calculation from precipitation modelling offers an efficient tool for time saving process development for a given application.
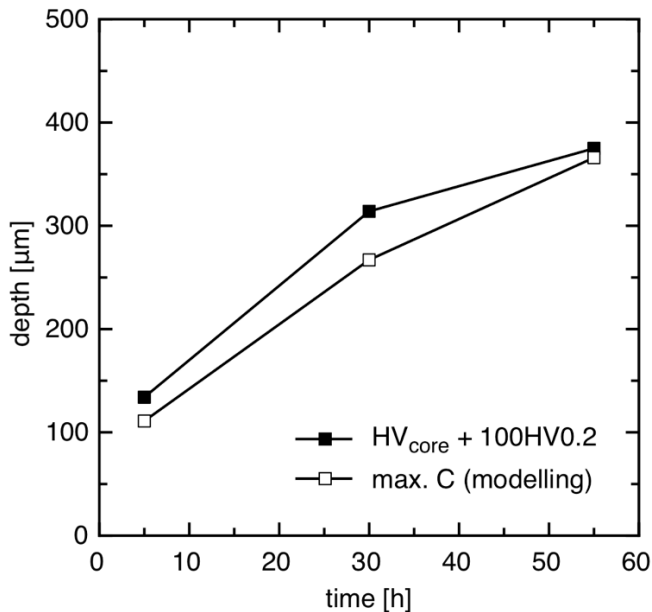

Figure 16: Comparisons between the experimental effective depth and the location of the maximum carbon content from modelling of a 33CrMoV12-9 steel nitrided at 520 °C and 3.65 atm$^{-1/2}$. The effective depth of nitriding is defined as the core hardness plus 100 HV 0.2.

Conclusions

Results from a model of nitriding of carbon low-alloyed steel was presented. Good agreements are obtained with experimental nitriding of a 33CrMoV12-9 steel grade under several treatment conditions (time, temperature and nitriding potential). The model is based on Fick's laws and thermodynamics calculations. It allows the prediction of the chemical in-depth gradients of both nitrogen and carbon as well as the fraction of phases. A method for determining the effective depth of nitriding is proposed based on consistency with the diffusion of carbon at the nitrogen diffusion front. Tuning nitriding conditions is then worth considering for a given effective depth.

References

[1] C.H. Knerr, T.C. Rose, and J.H. Filkowski, Gas Nitriding, *Heat Treating*, Vol. 4, ASM Handbook, ASM International, 1991, pp.387-409.

[2] S. Jegou, L. Barrallier, R. Kubler, M.A.J. Somers, Evolution of residual stress in the diffusion zone of a model Fe-Cr-C alloy during nitriding, *HTM J. Heat Treatm. Mat.*, Vol. 66, No. 3 (2011), pp.135-142.

[3] G. Fallot, S. Jegou, L. Barrallier, Evolution of residual stresses during short time nitriding of 33CrMoV12-9 steel grade, Advanced Materials Research, Vol. 996 (2014), pp.544-549.

[4] M. Le, F. Ville, X. Kleber, J. Cavoret, M.C. Sainte-Catherine, L. Briancon, Influence of grain boundary cementite induced by gas nitriding on the rolling contact fatigue of alloyed steels for gears, *Proc IMechE Part I: J Engineering Tribology*, Vol. 229, No. 8 (2015), pp.917-928.

[5] V.A. Phillips, A.U. Seybolt, A transmission electron microscopic study of some ion-nitrided binary iron alloys and steels, *Transaction of the Metallurgical Society of AIME*, Vol. 242 (1968), pp.2415–2422.

[6] B. Mortimer, P. Grieveson, K.H. Jack, Precipitation of nitrides in ferritic iron alloys containing chromium, *Scandinavian Journal of Metallurgy*, Vol. 1 (1972), pp203–209.

[7] K.H. Jack, Nitriding, *Heat Treatment*, No. 4 (1973), pp.39–50.

[8] M.A.J. Somers and E.J. Mittemeijer, Layer-growth kinetics on gaseous nitriding of pure iron : Evaluation of diffusion coefficients for nitrogen in iron nitrides, *Metallurgical and Materials Transactions A*, Vol. 26A (1995), pp.57–74.

[9] H. Du, J. Agren, Theoretical treatment of nitriding and nitrocarburizing of iron, *Metallurgical and Materials Transactions A*, Vol. 27A, No. 4 (1996) , pp.1073-1080.

[10] Y. Sun, T. Bell, A numerical model of plasma nitriding of low alloy steels, *Materials Science and Engineering*, Vol. A224 (1997), pp.33–47.

[11] M.A.J. Somers, Modelling nitriding of iron : from thermodynamics to residual stress, *Journal de Physique IV*, No. 120 (2004), pp.21–33.

[12] C. Ginter, L. Torchane, J. Dulcy, M. Gantois, A. Malchere, C.Eesnouf, T. Turpin, A new approach to hardening mechanisms in the diffusion layer of gas nitrided-alloyed steels. Effects of chromium and aluminium : experimental and simulation studies, *La metallurgia italiana*, Vol. 7-8 (2006), pp.29–35.

[13] J-N. Locquet, R. Soto, L. Barrallier, A. Charaï , Complete investigation of a nitrided layer for Cr alloy steel, *Microscopy Microanalysis Microstructures*, Vol. 8 (1997), pp.335-352.

[14] S. Jegou, L. Barrallier, R. Kubler, Phase transformation and induced volume changes in a nitrided ternary Fe-3%Cr-0.345%C alloy, Acta Materialia, Vol. 58 (2010), pp.2666-2676.

[15] D. Gunther, F.T. Hoffmann, T. Hirsch, P. Mayr, In-Situ measurements of residual stresses of chromium alloyed steels during a nitriding process, *ASM International 20th Heat Treating*, 9-12 October 2000.

[16] L. Torchane, P. Bilger, J. Dulcy, M. Gantois, Cinétique de croissance des couches en système polyphasé : Application aux systèmes Fe-N et Fe- N-C, *Entropie*, No. 202/203 (1997), pp.45–49.

[17] P. Depouhon, J.M. Sprauel, E. Mermoz, Prediction fo residual stresses and distortions induced by nitriding of complex 3D industrial parts, *CIRP Annals – Manufacturing Technology*, Vol. 64 (2015), pp.553-556.

[18] L. Barrallier, J.-C. Chaize, Modélisation des contraintes résiduelles dans les couches nitrurées de nuance 32CDV13, In *MAT-TEC 90, Grenoble, France*, October 1990, pp.83–88.

[19] L. Barrallier, Genèse des contraintes résiduelles de nitruration, Etude expérimentales et modélisation, PhD Thesis, Arts et Métiers ParisTech, France (1992).

[20] L. Barrallier, J. Barralis, On kinetics of gas nitriding : Case of steel, In *SMT8, Nice, France*, September 1994, pp. 621–625.

[21] S. Jegou, Influences des éléments d'alliage sur la genèse des contraintes résiduelles d'aciers nitrurées, PhD Thesis, Arts et Métiers ParisTech, France (2009).

[22] S. Jegou, R. Kubler, L. Barrallier, F. Roch, On residual stresses development during nitriding of steel: Thermochemical and time dependence. *Advanced Materials Research*, Vols. 89-91 (2010), pp.256–261.

[23] L. Barrallier, *Classical nitriding of heat treatable steel*, *Thermochemical Surface Engineering of Steels, Chapter 10,* Metals and Surface Engineering, Woodhead Publishing, 2014, pp.392–411.

[24] J.O. Andersson, T. Helander, L. Höglund, P.F. Shi, B. Sundman, Thermo-Calc and DICTRA, Computational tools for materials science, *Calphad*, Vol. 26 (2002), pp.273-312.

[25] Thermo-Calc Software TC-API User's Guide version 7.0, (Accessed 19 June 2014).

[26] Thermo-Calc Software TCFE7 Steels/Fe-alloys database version 7.0, (Accessed 23 Aug 2013).